

RECORD COPY
C.1

SANDIA REPORT

SAND90-2727 • UC-705

~~Unclassified Controlled Nuclear Information~~

Printed May 1991

UNCLASSIFIED
UNCONTROLLED

Ground Shock From Multiple Earth Penetrator Bursts: Effects for Small Weapon Arrays in Homogeneous Targets

L. N. Kmetyk, P. Yarrington

Prepared by
Sandia National Laboratories
Albuquerque, New Mexico 87185 and Livermore, California 94550
for the United States Department of Energy
under Contract DE-AC04-76DP00789

SNLA LIBRARY



* 8 3 8 5 3 4 4 *

SAND90-2727
0001
UNCLASSIFIED

05-91
45P STAC

~~UNCLASSIFIED CONTROLLED NUCLEAR INFORMATION NOT FOR PUBLIC DISSEMINATION~~

May contain unclassified controlled nuclear information subject to Section 148 of the Atomic Energy Act as amended (50 USC 2168). Approval by the Department of Energy prior to release is required.

DOES NOT CONTAIN UCNI

DEPARTMENT OF ENERGY DECLASSIFICATION REVIEW	
1ST REVIEW DATE: 2-21-96	DETERMINATION (CIRCLE NUMBER(S))
AUTHORITY: EADG EADG X-00	1. CLASSIFICATION RETAINED
NAME: <i>PH Squires</i>	2. CLASSIFICATION CHANGED TO:
2ND REVIEW DATE: 9/1/05	3. CONTAINS NO DOE CLASSIFIED INFO
AUTHORITY: ADD	4. RECLASSIFY WITH:
NAME: <i>Nancy Connolly</i>	5. CLASSIFICATION CANCELLED
	6. CLASSIFIED INFO STRIPPED
	7. OTHER (SPECIFY): <i>confirm unclassified</i>

HRP schmitt 5/11/07 DOES NOT CONTAIN UCNI

877

45 P

Ground Shock from Multiple Earth Penetrator Bursts: Effects for Small Weapon Arrays in Homogeneous Targets

L.N.Kmetyk

P.Yarrington

Computational Physics & Mechanics Division

Sandia National Laboratories

Albuquerque, New Mexico 87185

Abstract

Calculations have been performed with the HULL hydrocode to study ground shock effects for two- and three-burst earth penetrator weapon (EPW) arrays in a homogeneous target geology. Several different multiburst problems are described in this report. The first simulations involved a two-burst array assumed to be fully-contained (*i.e.*, at infinite DOB), and showed regions of substantial enhancement of ground shock over that of a single burst. Different weapons spacings with both simultaneous and non-simultaneous burst timing were considered. Three-dimensional calculations were done to model a two-burst array at 7m DOB and a three-burst array at 15m DOB. Results of the calculations again indicate that the multiburst array would enhance ground shock effects over those for a single burst in certain regions of the target. The 3D calculations also provided detailed information on the 3D lethal contours produced by such arrays.

Contents

1. Introduction	7
2. Source and Target Material Modeling	11
3. Fully-Contained, 2-Burst Calculations	13
3.1 Calculational Model	13
3.2 Baseline Study	15
3.3 Sensitivity Studies: Array Spacing and Timing	19
3.4 Comparison to LANL Multiburst Analyses	19
4. Finite Depth-of-Burst Calculations	25
4.1 Two-Burst Array at 7m-DOB – Computational Model	25
4.2 Two-Burst Array at 7m-DOB – Results	26
4.3 Three-Burst Array at 15m-DOB – Computational Model	26
4.4 Three-Burst Array at 15m-DOB – Results	30
5. Discussion and Conclusions	39
References	41
Appendix A. Results Archival	43
 Tables	
2.1 HULL Material Property Data	12
3.1 Problem Time, Burst Distance and Cell Size for the Transition from a Single Independent Burst to Two Interacting Bursts for the Different Weapon Spacings Considered in the Study	15

Figures

1.1	Geometry for Two-Burst and Three-Burst EPW Arrays	8
3.1	Use of Single-Burst Result to Generate Starting Conditions for Calculations of Two, Simultaneous, Fully-Contained Bursts	14
3.2	Use of Single-Burst Results to Generate Starting Conditions for Calculations of Two, Non-Simultaneous, Fully-Contained Bursts	16
3.3	Pressure Contours for Two, Simultaneous, Fully-Contained 100kt Bursts at 200m Separation	17
3.4	Peak Pressure Contours for Fully-Contained Single Burst and Multiburst Array	18
3.5	Peak Pressure Contours for Two, Simultaneous, Fully-Contained 100kt Bursts at Various Separation Distances	20
3.6	Pressure Contours for Two, Fully-Contained, Non-Simultaneous 100kt Bursts at 200m Separation	21
3.7	Peak Pressure Contours for Two, Fully-Contained, Simultaneous and Non-Simultaneous 100kt Bursts at 200m Separation	22
3.8	Peak Pressure Contours for Two, Non-Simultaneous, Fully-Contained 100kt Bursts from LANL and SNL Studies	23
4.1	Use of Single-Burst Result to Generate Starting Conditions for 3D Calculations of Two, Simultaneous Bursts at 7m-DOB	27
4.2	Pressure Contours for Two, Simultaneous 100kt Bursts at 7m-DOB and 200m Separation	28
4.3	Peak Pressure Contours for Two, Simultaneous 100kt Bursts at 7m-DOB and 200m Separation	29
4.4	Use of Single-Burst Result to Generate Starting Conditions for 3D Calculations of Three, Simultaneous Bursts at 15m-DOB	31
4.5	Pressure Contours at 100ms for Three, Simultaneous 100kt Bursts at 15m-DOB and 200m Separation	32
4.6	Pressure Contours at 250ms for Three, Simultaneous 100kt Bursts at 15m-DOB and 200m Separation	33
4.7	Peak Pressure Contours on Horizontal Planes for Three, Simultaneous 100kt Bursts at 15m-DOB and 200m Separation	35
4.8	Peak Pressure Contours on Vertical Coordinate Planes for Three, Simultaneous 100kt Bursts at 15m-DOB and 200m Separation	36
4.9	Comparison of Peak Pressure Results for Single (300kt) Burst and Multiburst (3-100kt) Array	37

1. Introduction

There exists a class of strategic targets which, because of their great depth, cannot be credibly held at risk with surface burst weapons. Calculations suggest that severe damage can be inflicted on these targets, however, by ground shock from earth penetrator weapons (EPWs) of moderate yield (see, *e.g.*, [1]). Under certain circumstances, it may be necessary or desirable to deploy a number of small yield devices in order to achieve the desired ground shock effects against these targets.

A spaced array of EPW bursts, detonated simultaneously, could be expected to produce enhanced ground shock effects when compared with effects from an equal number of identical bursts detonated *independently*, *i.e.*, over a time period too long to allow burst interaction. Ground shock effects from the multiple, synchronized bursts might, in fact, be comparable to those from a single burst of the same total yield (or same *aggregated yield*) as that of the array. There is little data, however, on ground shock effects from multiple, buried bursts to make these evaluations, and testing programs at representative scale would be quite expensive. Thus, calculational simulation techniques, which can be employed at a fraction of the cost of field testing, provide an attractive option for investigating the relative effects of single and multiple EPW bursts.

This report presents HULL [2] hydrocode calculations of ground shock from detonations for two-burst and three-burst arrays of earth penetrator weapons in a homogeneous target material. As illustrated in Figure 1.1, the EPWs were assumed to be either a separated pair of bursts or three bursts at the vertices of an equilateral triangle. Each burst in the array was assumed to have a nominal yield of 100kt, and the target material was assumed to be a homogeneous, wet, soft rock. The source and target modeling are discussed in Section 2.

Ground shock effects have been simulated for: 1) two fully-contained bursts, *i.e.*, at infinite depth-of-burial (DOB), and 2) two-burst and three-burst arrays at finite DOB. The advantage of assuming full containment of the bursts is that it allows multiburst ground shock analyses with simpler and faster two-dimensional (2D) calculations, rather than requiring full three-dimensional (3D) simulations. The 2D calculations can be used to explore multiburst wave interaction effects and sensitivities to certain problem parameters, *e.g.*, weapon spacing and timing; however, the quantitative results cannot be related easily to realistic EPW problems.

Section 3 presents calculational results for two fully-contained EPW bursts. Calculations were done for single bursts, pairs of simultaneous bursts at different separation distances, and a pair of bursts detonated non-simultaneously. These results are compared with a series of similar calculations done by LANL using the SHALE code [2]. The LANL

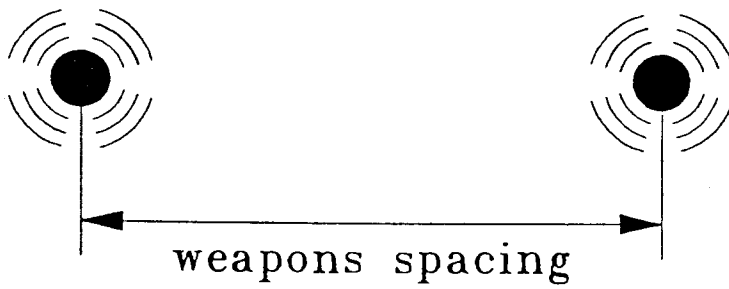
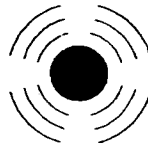
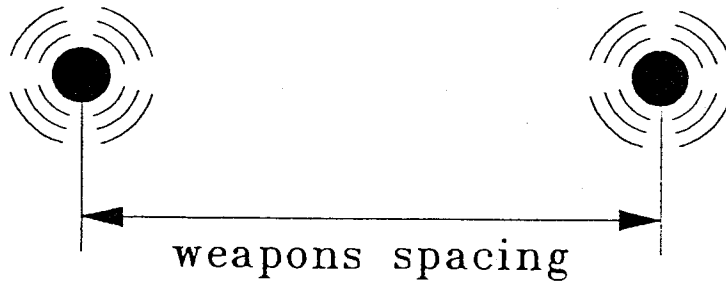


Figure 1.1. Geometry for Two-Burst (top) and Three-Burst (bottom) EPW Arrays

study analyzes two simultaneous 500kt bursts [3] and two non-simultaneous 100kt bursts [4], with different weapon spacings and timings.

Three-dimensional HULL calculations were also done for two-burst and three-burst arrays, at 7m-DOB and 15m-DOB, respectively. The results of those calculations are presented in Section 4. Note that the 7m DOB problem was chosen, for comparison purposes, to be at the same scaled DOB as an earlier calculation [1] of a 500kt EPW burst at 12m DOB. Finally, Section 5 provides a summary of the study and its conclusions. The input listings and code changes used for the calculations are given in the Appendix, along with file storage information, for reference.

2. Source and Target Material Modeling

The HULL code system [1] consists of a set of computer programs for generating and solving continuum dynamics problems, plus assorted programs such as are required, for example, to produce plots. As currently configured, HULL solves two- and three-dimensional Eulerian and Lagrangian problems, and provides various means for linking these two types of solutions. For the present study, all calculations were run in the Eulerian mode.

The energy release of each EPW burst was modeled in the calculations by instantaneously depositing the yield of the weapon (*i.e.*, 100kt) in a 1m-radius sphere of the geologic target material centered at the weapon position. The target material was assumed to be uniform and undisturbed in all directions surrounding each burst point. For deeply-buried bursts, such as those considered here, energy transfer by radiation transport should be insignificant and was not included in the calculations.

Virtually all material property data (except air) are read from an extensive material library file (MATLIB). Air is modeled in the code with an inline equation-of-state (EOS). The MATLIB file includes the EOS of the material and its strength properties. The user can change the basic data for a material or add new materials, as long as they can be represented by one of the EOS types in MATLIB. For the present simulations, the ground material was modeled with the Mie-Gruneisen EOS, and Table 2.1 lists the material constants that were used. Material strength effects were ignored in these calculations.

The automatic rezoning logic in the HULL program was substantially modified for the present calculations, in large part to ensure that both two- and three-dimensional analyses used exactly the same mass-, momentum- and internal-energy-conserving rezone scheme. A listing of the rezone change deck used for the present calculations is included in the appendix, for reference.

The automatic rezoning used in the present calculations expanded the mesh as the shock front grew radially outward from the bursts. The rezone was "triggered" by a non-zero velocity and/or non-ambient pressure in any cell adjacent to the outer boundary of the mesh. When triggered, the expanding rezoner increased the cell size in every direction by 5%, holding fixed any reflecting boundary (*e.g.*, $x=0$). As the cells expanded beyond the original mesh, they were filled with tuff and/or air at ambient conditions, as determined by the cell location.

material property data for material named air
 ambient density = 1.2250e-03
 ambient sound speed = 3.4029e+04
 ambient energy = 2.0679e+09
 gamma = 1.4000e+00
 units are assumed to be cgs

material property data for material named mtuff
 ambient density = 2.0000e+00
 ambient sound speed = 2.8000e+05
 shock vel/particle vel slope = 1.0100e+00
 gruneisen ratio = 1.0000e+00
 minimum pressure = -1.0000e+08
 poissons ratio = 2.5000e-01
 rigidity modulus = 9.4080e+10
 atomic weight = 0.6000e+02
 debye temperature = 0.3800e+03
 vapor state coefficient = 0.2500e+00
 ambient energy = 0.6798e+09
 ambient melt energy = 0.1000e+11
 fusion energy = 0.8000e+10
 sublimation energy = 0.1200e+12
 energy at beginning of vapor = 0.5000e+11
 energy at end of vapor = 0.1000e+12
 initial yield strength = 1.0000e+09
 maximum yield strength = 1.0000e+09
 strain at maximum yield = 3.0000e-01
 thermal softening coeff yf1 = 9.0000e-01
 thermal softening coeff ef1 = 9.0000e-01
 thermal softening coeff yf2 = 9.0000e-01
 thermal softening coeff ef2 = 9.0000e-01
 principal stress at failure = 0.1000e+21
 principal strain at failure = 0.1000e+21

units are assumed to be cgs

Table 2.1. HULL Material Property Data

3. Fully-Contained, 2-Burst Calculations

Two EPW bursts, detonated deep enough in a homogeneous medium for the ground shock to be considered fully-contained, can be analyzed using 2D axisymmetric calculations, where the bursts are positioned at the appropriate separation distance along the axis of symmetry. The results of such calculations, as described in this section, can provide insights to the burst interaction phenomenology and can be used to evaluate problem parameter sensitivities, for example, weapon spacing and differences in burst timing, or "jitter".

3.1 Calculational Model

Calculations for the two fully-contained simultaneous bursts were initiated from intermediate results of a calculation for a single burst centered at the origin ($x=0, y=0$). The single burst calculation used a grid of 200×400 square zones (in the radial and axial directions, respectively), with the cells initially 5cm on a side. The initial grid, therefore, covered a $10\text{m} \times 20\text{m}$ region of the target. The $x=0$ axis of symmetry is treated as a reflecting boundary in 2D cylindrical coordinates.

The expanding rezoner was used to follow the shock front in the single burst calculation until it reached a distance slightly less than half the weapon spacing desired for the two-burst array. That calculation was then stopped and the FIREIN option in HULL was used to move the burst position from the origin to its desired location for the two-burst problem, *i.e.*, to a y -position of half the weapon spacing desired. This process is illustrated in Figure 3.1, for one particular case, with 3.1(a) showing the single-burst configuration and 3.1(b) showing the single burst result displaced relative to the $y=0$ symmetry boundary to represent the two-burst problem.

The calculations were then resumed with the expanding rezoner used as before to follow the expanding shock front. An (x - y) grid of 200×200 square cells was used for the two-burst calculations. Table 3.1 summarizes the times, burst distances, and "initial" (*i.e.*, at the time of transition from a single-burst to a two-burst problem) for the different weapon spacings considered.

An additional 2D, fully-contained, two-burst calculation was done with the two bursts assumed to be detonated at different times (*i.e.*, with a 20ms timing jitter). This analysis was done with a 200×400 grid and with no symmetries assumed in the interaction region. As indicated in Table 3.1 and Figure 3.2, two different edits from the original single-burst calculation were inserted, using the FIREIN option, at two different y locations, just prior to the time that ground shock interaction would begin. Figure 3.2

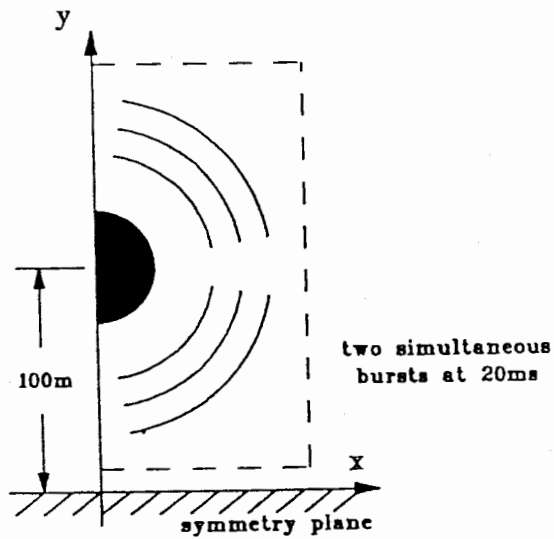
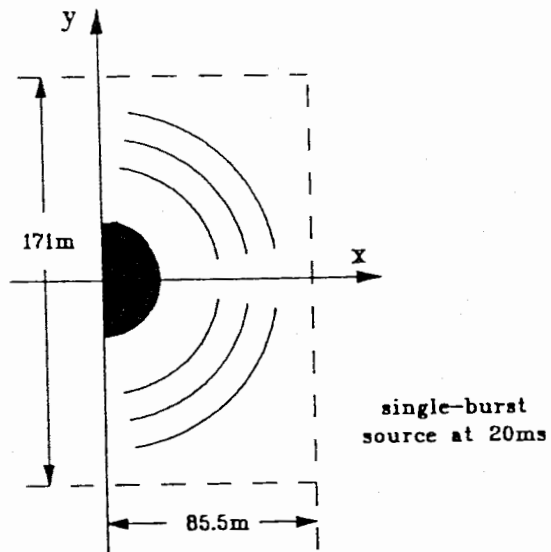


Figure 3.1. Use of Single-Burst Result (top) to Generate Starting Conditions (bottom) for Calculations of Two, Simultaneous, Fully-Contained Bursts

Table 3.1. Problem Time, Burst Distance and Cell Size for the Transition from a Single Independent Burst to Two Interacting Bursts for the Different Weapon Spacings Considered in the Study

Weapon Spacing (m)	Transition Time(s) (ms)	Shock Radius (m)	Cell Size (cm)
50	2.94	24.0	25
100	8.80	47.5	50
200	20.0	85.5	100
500	70.0	248.0	250
200	10 & 30	52.5 & 120.0	100

illustrates the two different single-burst results used and the two single bursts displaced relative to a $y=0$ midpoint. The calculation was then resumed with the expanding rezoner used as before to follow the shock fronts outward.

3.2 Baseline Study

Figure 3.3 shows pressure contours for the ground shock interactions from two 100kt bursts, separated by a distance of 200m and detonated simultaneously. Figure 3.3a shows results at 100ms, shortly after first interaction of the shock fronts from the two bursts. Figure 3.3b shows later stages in the shock propagation and interaction process.

Peak pressure contours in a plane through the burst centers are shown in Figure 3.4a, for the 1 kb and 2 kb pressure levels. The 1 kb contour is compared in Figure 3.4b to the corresponding contour for a single 200kt fully-contained burst. As can be seen in these figures, there is a region on either side of the plane between the two synchronized 100kt bursts where ground shock is enhanced over that from a single 200kt burst. Elsewhere, the two smaller bursts generally deliver lower ground shock levels than the 200kt burst. In most areas of the target, the *peak* pressure levels are equivalent to those of a single 100kt burst, since the shock from the second burst arrives too late to interact significantly.

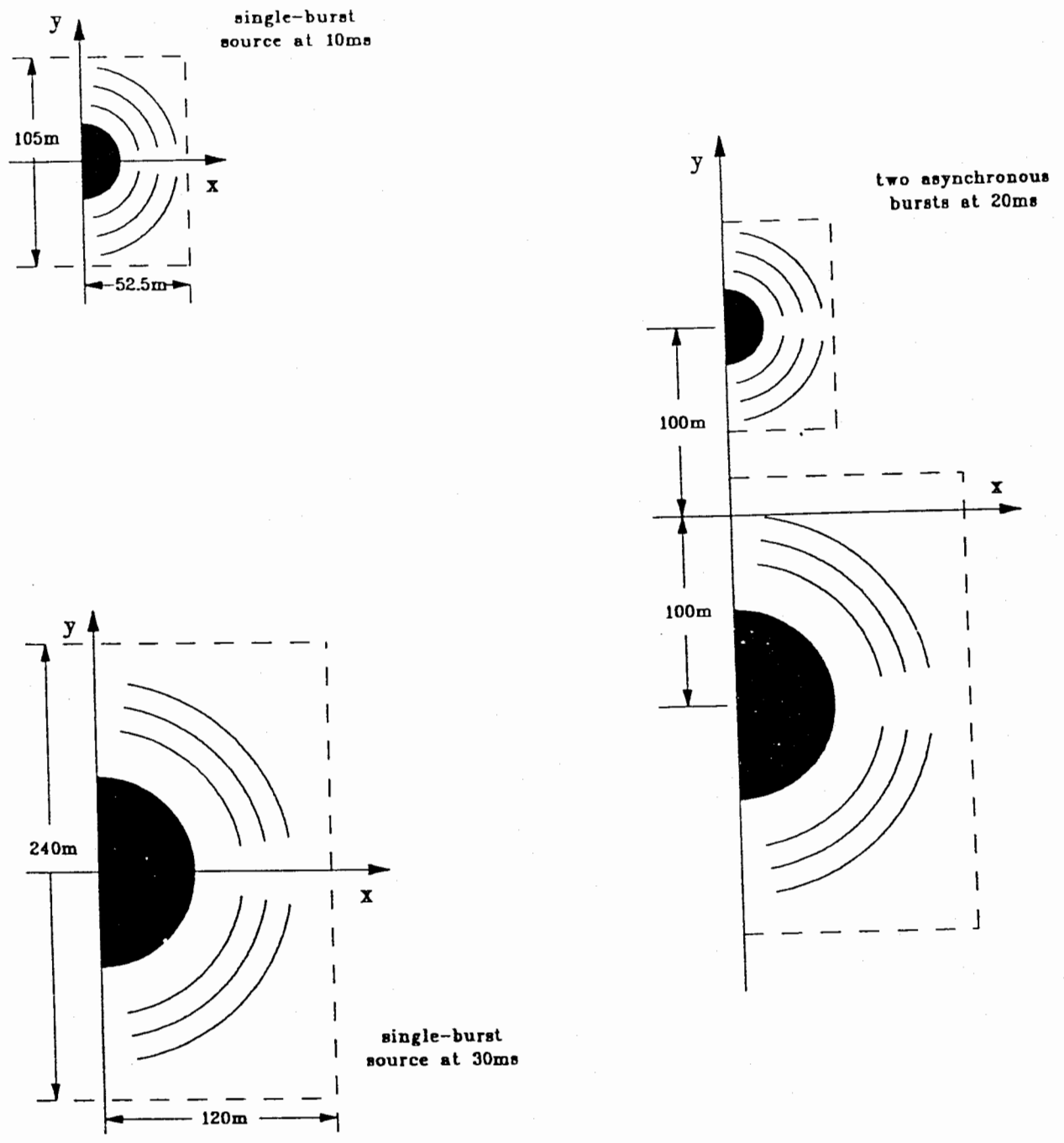


Figure 3.2. Use of Single-Burst Results (left) to Generate Starting Conditions (right) for Calculations of Two, Non-Simultaneous, Fully-Contained Bursts

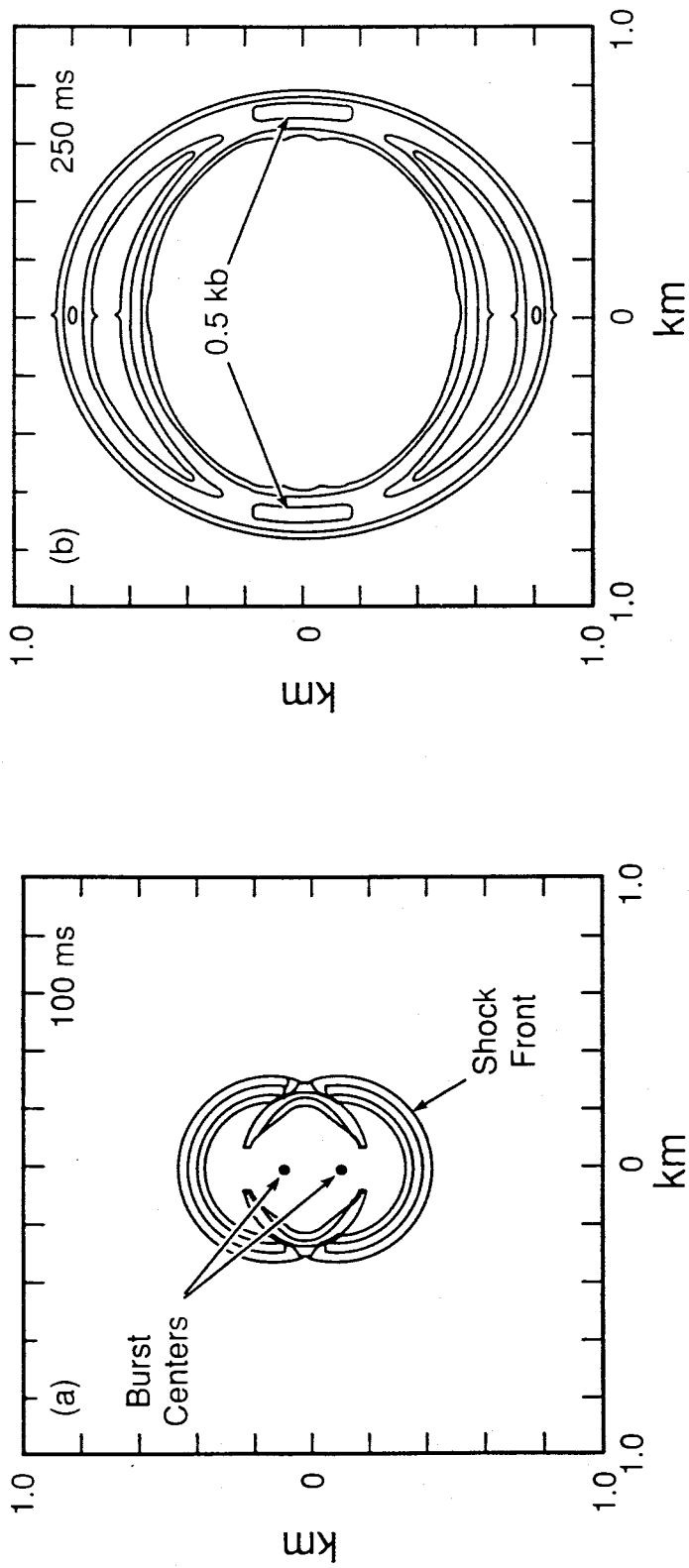


Figure 3.3 Pressure Contours on Plane Through Burst Centers for Two, Fully-Contained, Simultaneous 100 kt Bursts at 200 m Separation

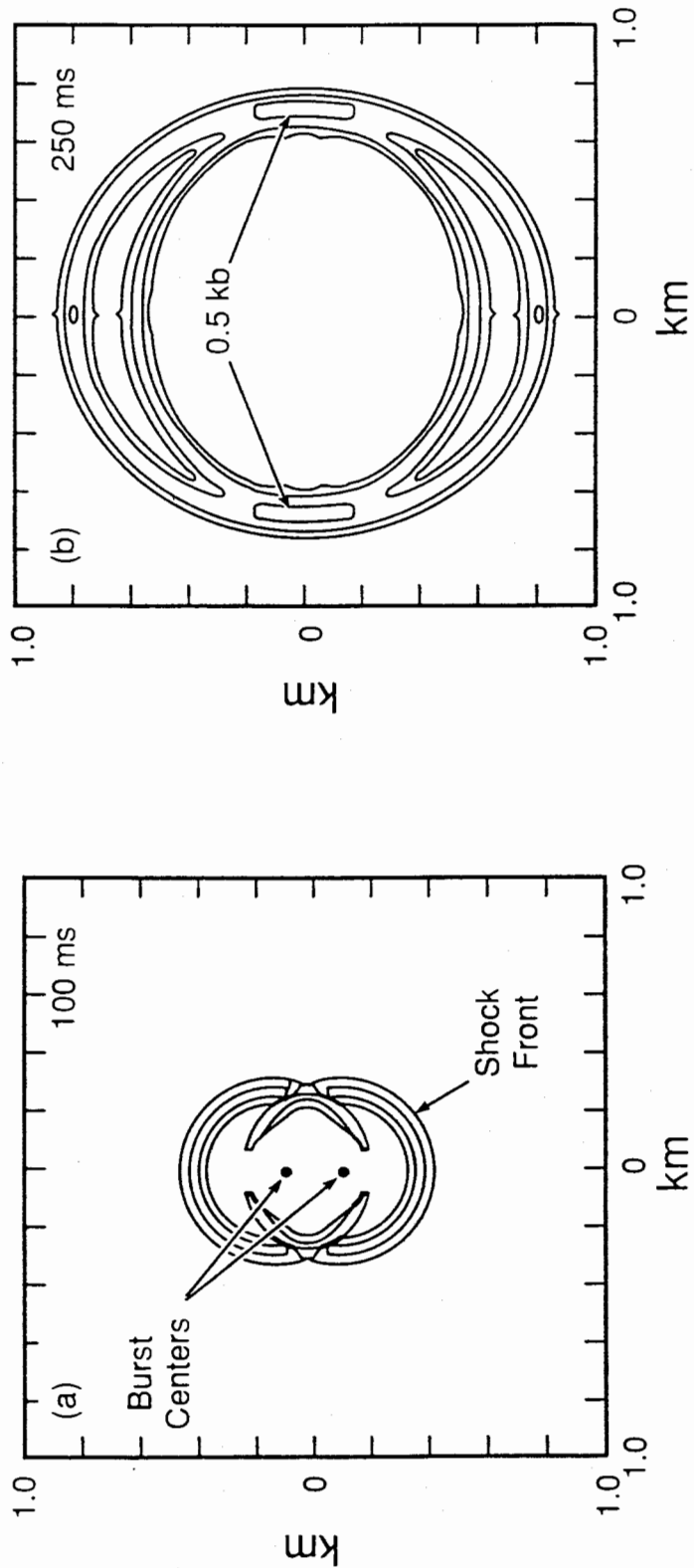


Figure 3.3 Pressure Contours on Plane Through Burst Centers for Two, Fully-Contained, Simultaneous 100 kt Bursts at 200 m Separation

3.3 Sensitivity Studies: Array Spacing and Timing

Spacing Study

In addition to the basecase weapon spacing of 200m, three other cases have been analyzed, corresponding to weapon spacings of 50, 100 and 500m. Figure 3.5 shows peak pressure contours in the plane of burst centers for these four cases. As would be expected, the region of ground shock enhancement between the two bursts is seen to decrease with an increase in weapon spacing. Thus, in terms of ground shock, bursts farther produce effects similar to two independent bursts, while bursts closer together produce effects similar to a single burst of the same total aggregated yield.

Timing Study

As described in Section 3.1, an additional 2D calculation was run in which the two 100kt bursts, separated by a distance of 200m (as in the baseline study), were detonated 20ms apart. The resulting pressure contours are shown in Figure 3.6. The plot times are the same as shown in Figure 3.3 for the case of simultaneous detonations. Figure 3.7 compares peak pressure contours on a plane through the burst centers for the baseline calculation and for the present non-simultaneous timing study. It can be seen that the timing jitter causes the region of constructive ground shock interaction and enhancement to shift toward the delayed burst.

3.4 Comparison to LANL Multiburst Analyses

Our 2D, fully-contained, two-burst array calculations can be compared with similar results obtained by Los Alamos National Laboratory (LANL) using the SHALE [2] code. The LANL analyses modeled two simultaneously-detonated 500kt bursts [3] and two non-simultaneously-detonated 100kt bursts [4], both in a homogeneous, infinite, limestone geology. The simultaneous-burst analyses by LANL considered both saturated and unsaturated (porous) target material, while their analyses of non-simultaneous-bursts considered only the saturated case. The different target material modeled in LANL calculations and the higher weapon yield used for one of the analyses (as well as code and zoning differences) preclude any but qualitative comparisons with results of the present study.

Figure 3.8a shows peak pressure contours for the LANL calculation [4] for two fully-contained 100kt bursts in saturated limestone, separated by 200m and detonated 20ms apart. Figure 3.8b compares the 1 kb peak pressure contours from the SNL and LANL studies. Qualitatively, both calculations are predicting a similar shift of the enhanced ground shock region toward the delayed burst. The small differences in shape and size of the contours may be easily attributed to the differences in geology between the two studies.

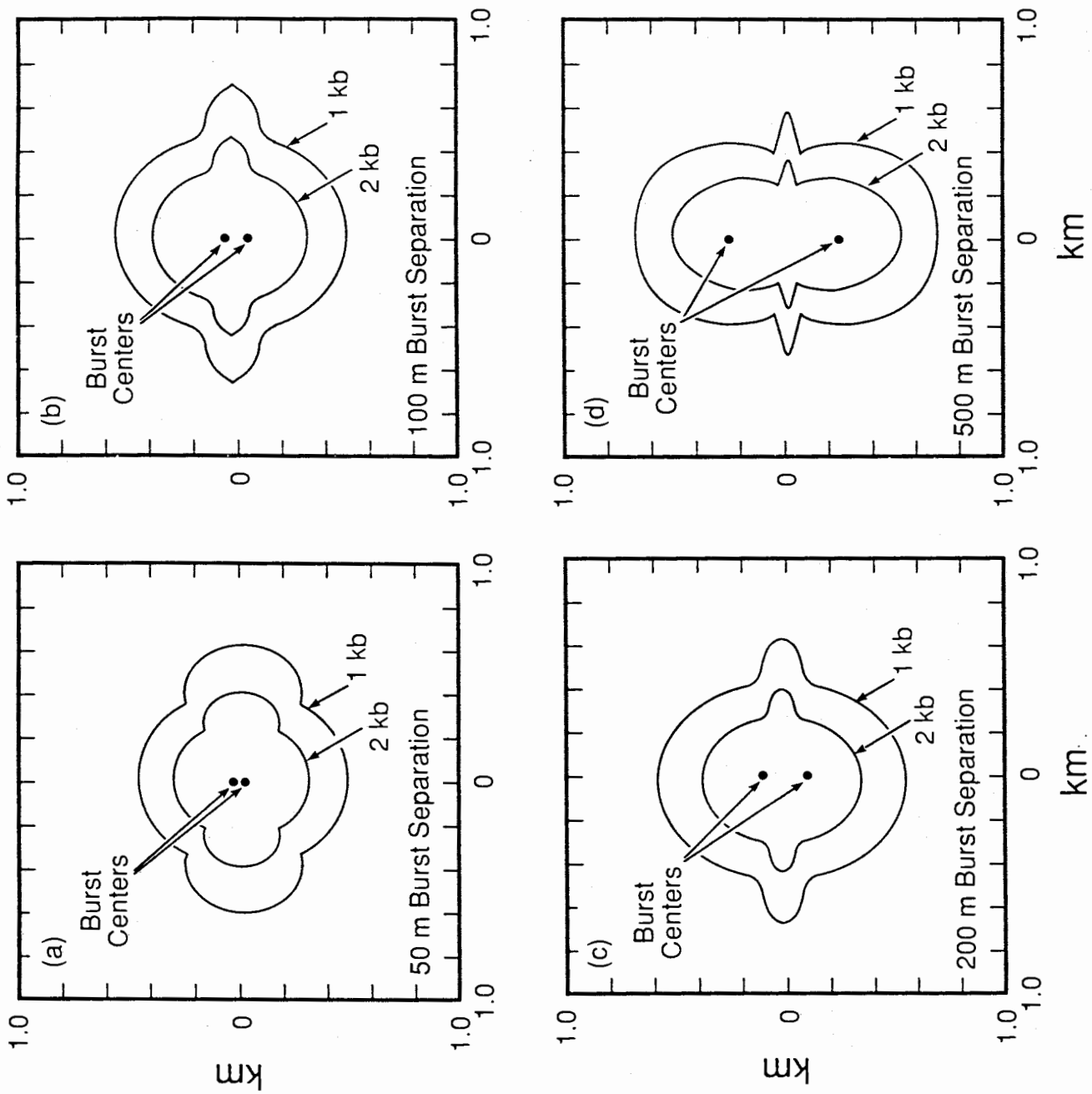


Figure 3.5 Peak Pressure Contours for Two, Simultaneous, Fully-Contained 100 kt Bursts at various Separation Distances

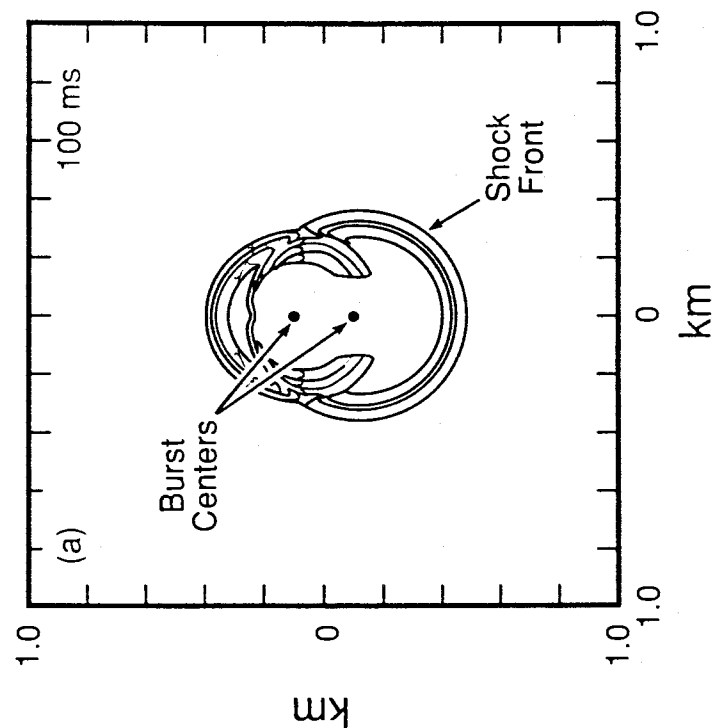
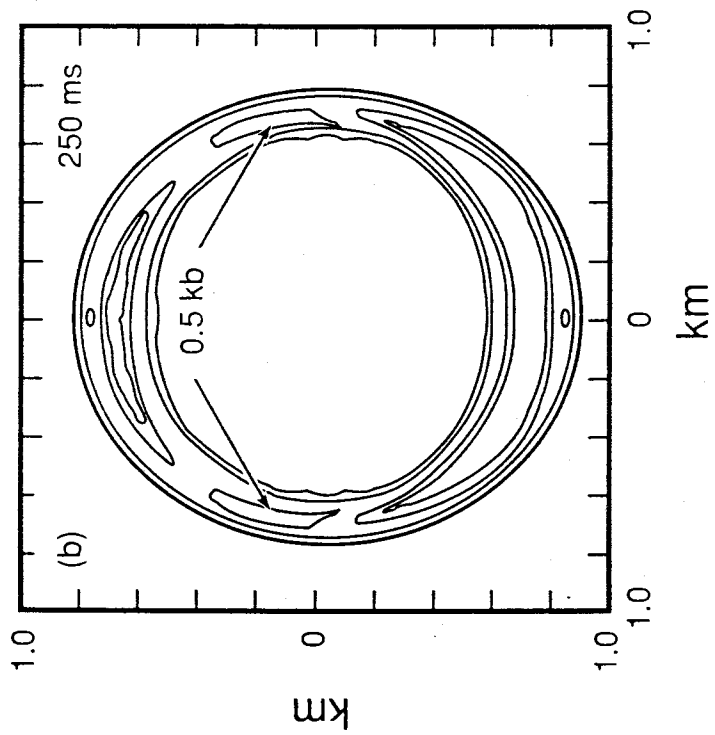


Figure 3.6 Pressure Contours on Plane Through Burst Centers for Two, Fully-Contained, Non-Simultaneous 100 kt Bursts at 200 m Separation

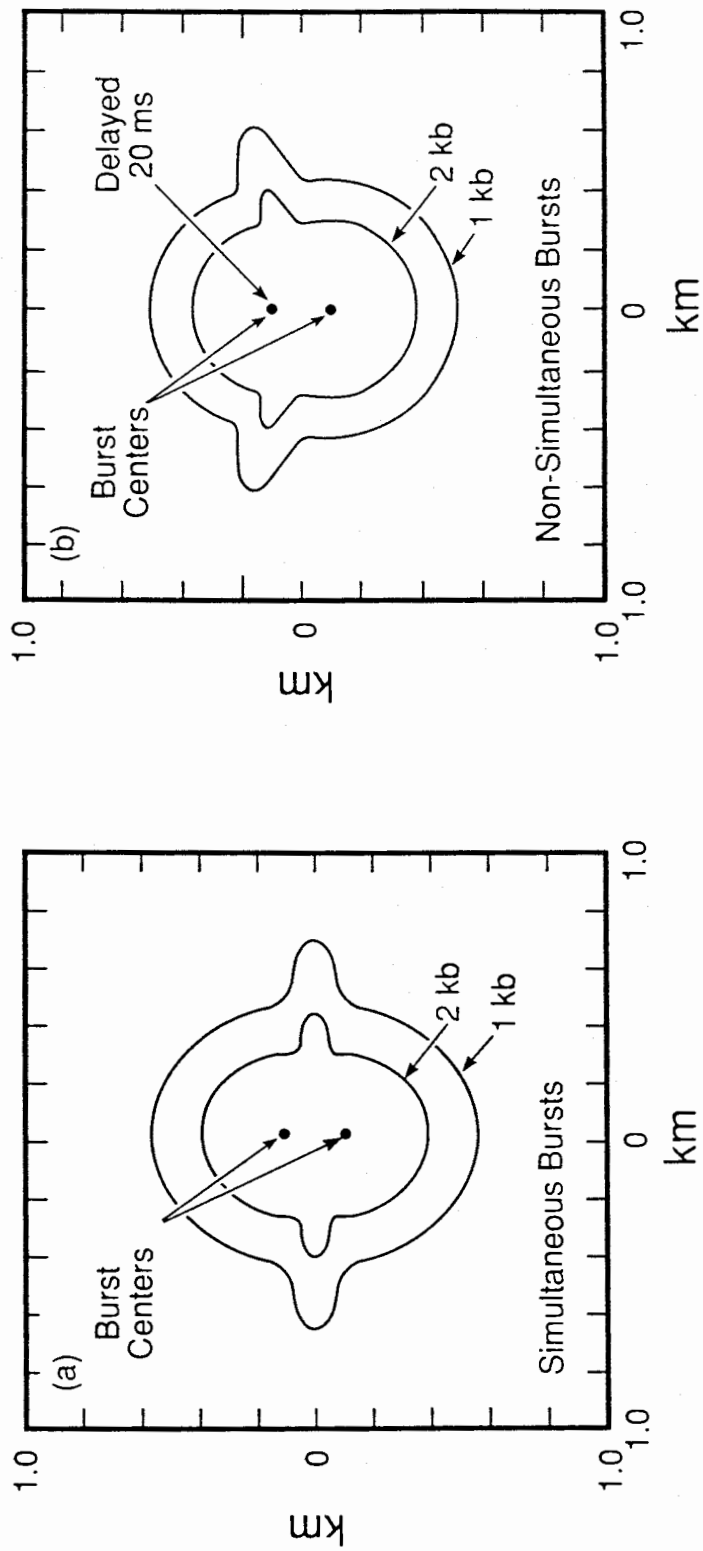


Figure 3.7 Peak Pressure Contours on Plane Through Burst Centers for Two, Fully-Contained 100 kt Bursts (Left: Simultaneous Bursts; Right: Non-Simultaneous Bursts)

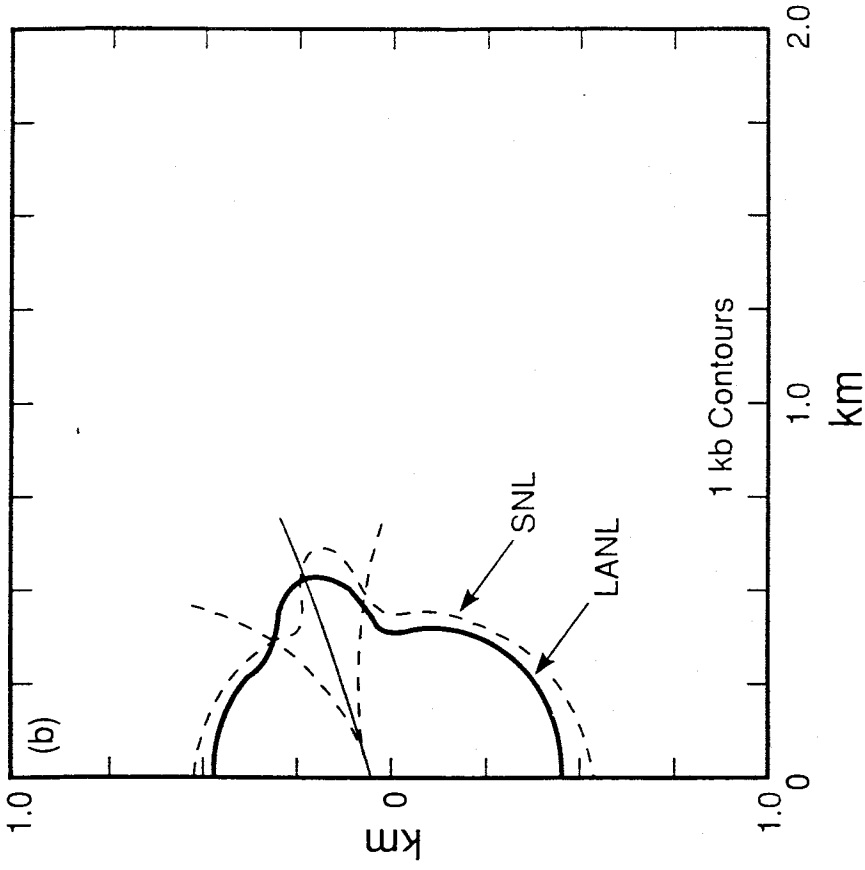
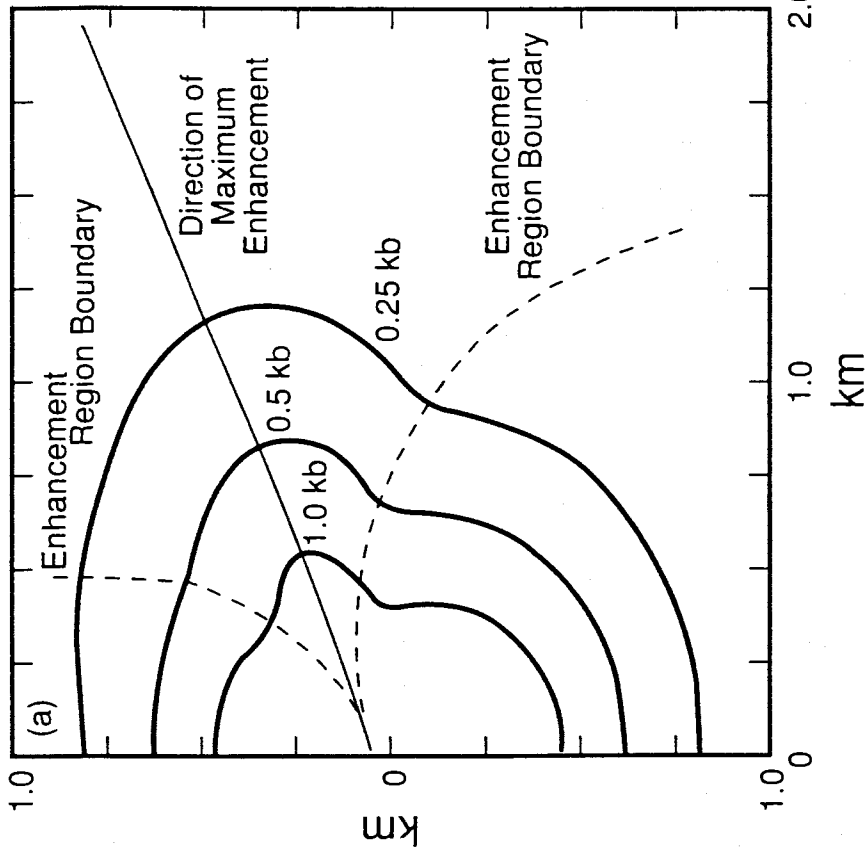


Figure 3.8 Peak Pressure Contours for Two, Fully-Contained, Non-Simultaneous Bursts
 (a) LANL Results Compared with LANL Analytic Method Prediction
 (b) LANL Results Compared with SNL Results

The LANL multiburst study [4] also presented an analytical technique based on linear superposition analysis for predicting how the region of enhancement varies with separation distance and timing differences for the two-burst problem. The curve of maximum constructive interference is analytically determined from the shock propagation velocity (found to be 3.41km/s at 50-100ms for the present calculation), and the curves that "bound" the region of constructive enhancement are determined from the leading and trailing shock pulse half-height velocities (3.65km/s and 3.13km/s, respectively, in the HULL calculation during the 50-100ms interval). The analytic predictions locating the region of ground shock enhancement in the LANL studies are shown in Figure 3.8a, while similar results using the LANL equations, together with wave velocities from the present HULL calculations, are shown in Figure 3.8b. The analytic results appear to predict well the direction and extent of the region of enhancement in both studies, suggesting that wave interaction phenomenology for the two burst problem is reasonably well represented by linear superposition of the waves.

4. Finite Depth-of-Burst Calculations

In addition to the 2D, fully-contained, two-burst analyses discussed in the last section, ground shock effects have been simulated for two- and three-burst arrays with the bursts at a finite DOB. Special computational techniques were required to treat the 3D problem of a multiburst array, such that adequate resolution is provided during all stages of the calculation without having computing costs be prohibitive. For the 3D finite array calculations in the present study, the HULL FIREIN option enabled this to be done.

In general, there is a period of time after detonation of weapons in a multiburst array when the shocks propagate independently of each other. This period of independent ground shock propagation depends, of course, on the timing and spacing of the bursts. During this initial phase of the problem, the bursts can clearly be modeled as separate, 2D axisymmetric events.

With the HULL FIREIN option, it is possible to insert results of separate 2D calculations for the individual bursts into the 3D grid before wave interactions have occurred. Variations in spacing and/or timing between bursts can be easily represented by selection of the appropriate time edits from the 2D calculation and by proper insertion, or placement, of these results in the 3D grid. The 3D mesh is created initially to be just large enough to the ground shock region from the bursts, immediately prior to interaction, and is then adjusted to follow the expanding shock waves using automatic rezoning techniques.

Two 3D calculations were done in the present study. One of these involved two 100kt bursts, separated by 200m and detonated simultaneously at 7m-DOB, and the other involved three 100kt bursts, spaced 200m apart and detonated simultaneously at 15m-DOB.

4.1 Two-Burst Array at 7m-DOB – Computational Model

A 2D 7m-DOB, single-burst calculation was performed to get initial conditions for the two-burst problem. This calculation used a 50×150 grid of square zones. The problem was begun with zones 10cm on each side, and the initial grid extended from the $x=0$ axis of symmetry outward radially for 10m. The corresponding axial region included 20m of target material and 10m of air above the burst, with $y=0$ representing the ground surface. The automatic, expanding rezoner option (as described in Section 2) was used to extend the initial zoning during the calculation to follow the expanding ground shock.

The 2D single burst calculation was run until the shock front reached a distance slightly less than half the weapon spacing desired for the two-burst problem. In the

present case, that distance was 100m, and the single burst calculation was stopped at 14.5ms, at which time the shock front had reached a radius of 97.5m. At that point, the FIREIN option was used to map the 2D results to the desired position in the 3D grid, as described below.

The initial three-dimensional mesh was constructed to be just large enough to contain the wave front from the single burst inserted in the grid. Due to the symmetry of the problem, it was possible to use reflecting boundary conditions at $x=0$ and $y=0$ and model only one quadrant of the problem, as shown in Figure 4.1. The 2D problem was then inserted in the 3D mesh with the burst center at 100m from the $x=0$ boundary. An (x,y,z) grid of $100 \times 50 \times 150$ cells was used, with cubical cells initially 2m on each side; the initial 3D mesh therefore extended $200\text{m} \times 100\text{m} \times 300\text{m}$, with 100m vertically in the ground (below $z=0$). Just as in the 2D calculations, the expanding rezoner was then used to extend the initial 3D zoning to follow the expanding shock front(s).

4.2 Two-Burst Array at 7m-DOB – Results

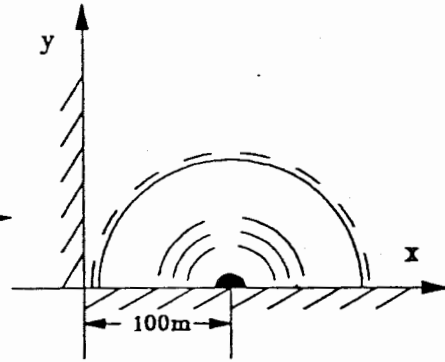
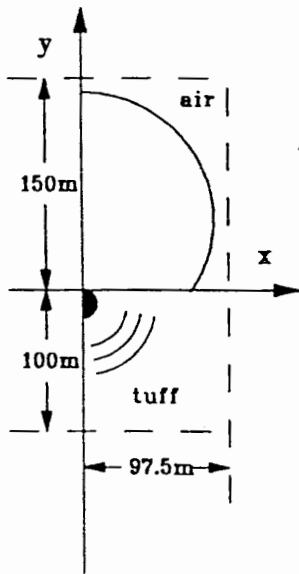
Pressure contours on a horizontal plane at 250m depth are shown in Figure 4.2a for two 100kt bursts at 7m DOB and 200m separation. Note that the highest pressures ($\sim 0.5\text{kb}$) in the plane at that time are on the vertical plane between the bursts. Figure 4.2b shows corresponding results for the pressure fields on vertical coordinate planes for the problem.

Information on the “footprint”, or area covered by a given level of ground shock, at various depths is required for assessing weapon effectiveness against buried targets. Figure 4.3a shows 0.5kb and 1.0kb footprints for the two-burst array on a target plane at $\sim 250\text{m}$ depth. It can be seen that a square region of $\sim 500\text{m} \times \sim 700\text{m}$ is covered by a pressure level of 0.5 kb, or greater. These results again clearly show the region of ground shock enhancement to be confined to a region near the plane between the bursts. Corresponding Peak pressure contours on vertical coordinate planes are shown in Figure 4.3b.

4.3 Three-Burst Array at 15m-DOB – Computational Model

For the three-burst problem, a 2D, 15m-DOB, single-burst calculation was done to establish initial conditions for the 3D calculation. This 2D single-burst calculation used a 100×300 mesh of square cells initially 10cm on each side. The initial mesh extended outward radially for 10m, while covering an axial region extending 20m into the ground and 10m into the air. The automatic, expanding rezoner option was used as already discussed to extend the initial zoning, until the shock front reached a distance slightly less than half the weapon spacing to be modeled in the three-burst problem. In this case, that distance was 100m, and the single burst calculation was stopped at 20ms, when the shock front had reached a radius of 90m. At that point, the HULL FIREIN option was

single 7mDOB burst
source at 14.5ms (2D)



(3D) two simultaneous
7mDOB bursts at 14.5ms

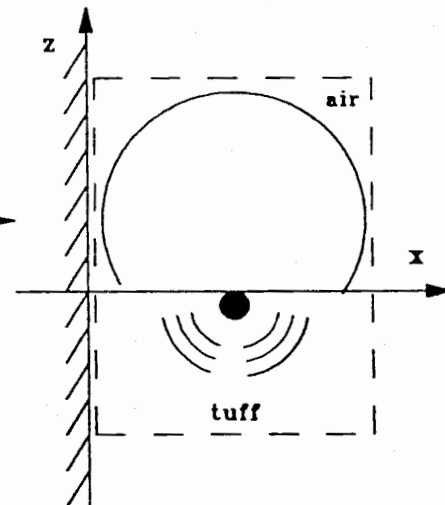


Figure 4.1. Use of Single-Burst Result (left) to Generate Starting Conditions (right) for 3D Calculations of Two, Simultaneous Bursts at 7m-DOB

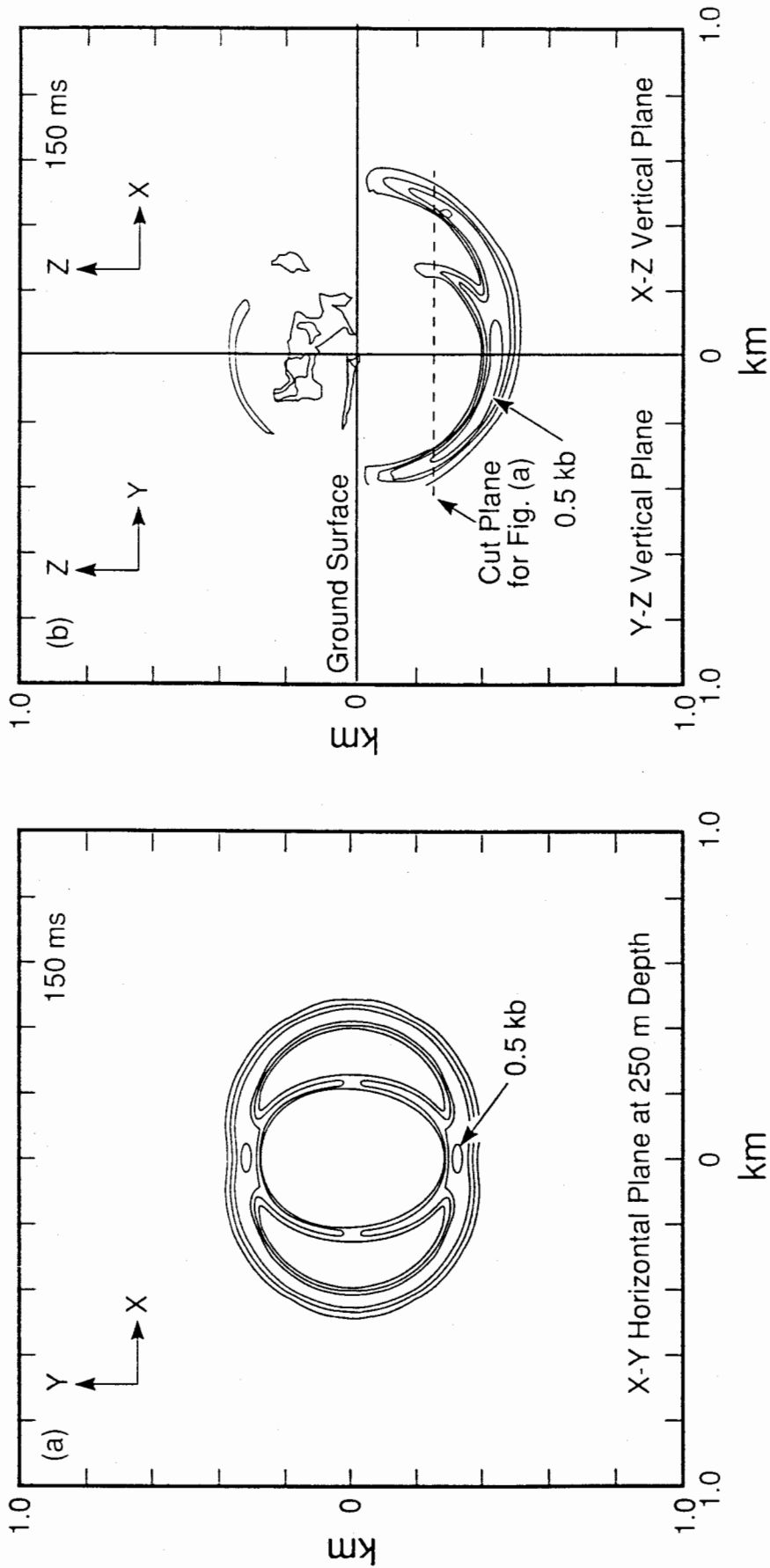


Figure 4.2 Pressure Contours for Two, Simultaneous, 100 kt Bursts at 7 m-DOB and 200 m Separation

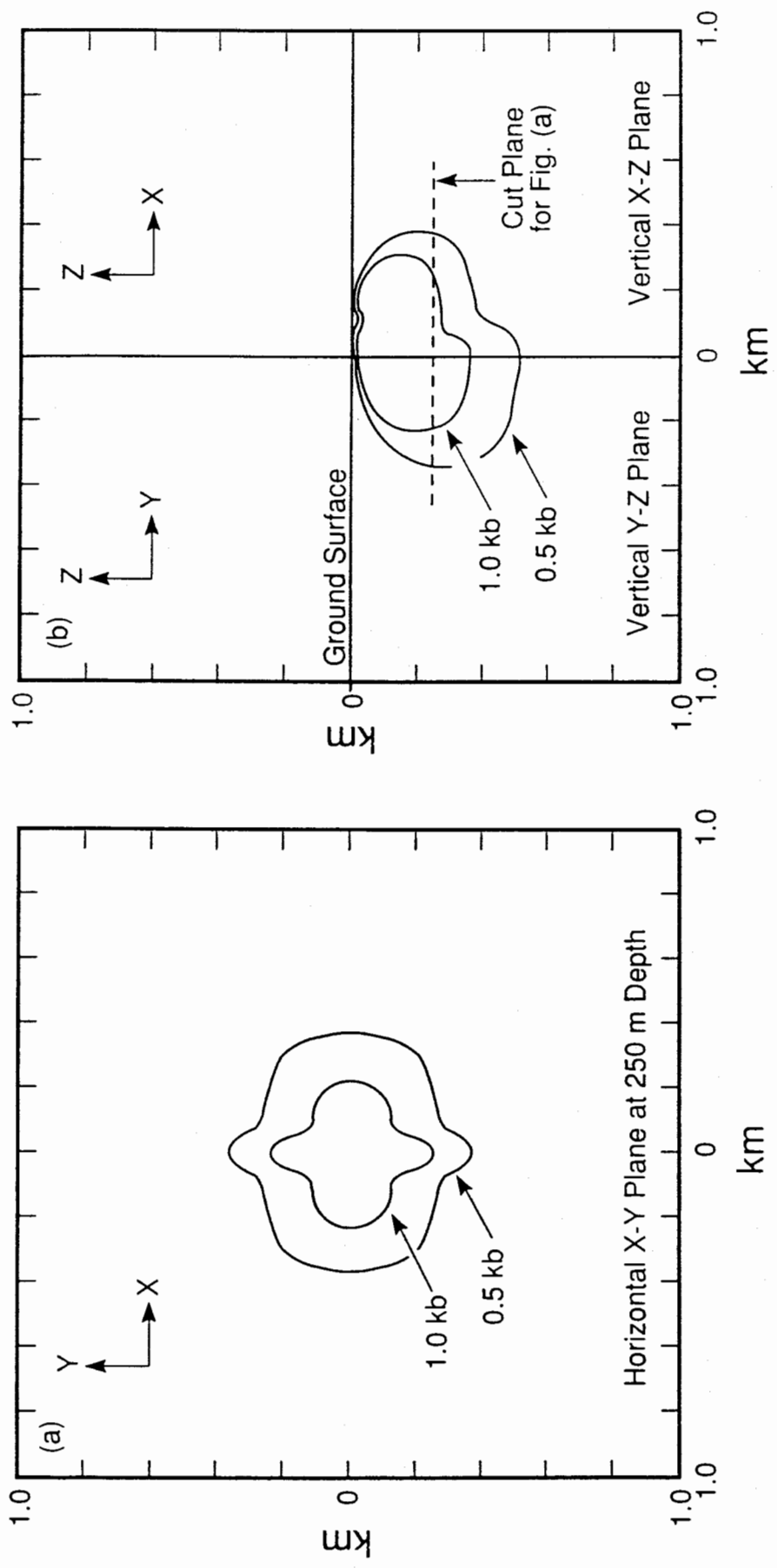


Figure 4.3 Peak Pressure Contours for Two, Simultaneous, 100 kt Bursts at 7 m-DOB and 200 m Separation

used to insert the single-burst result at two locations in the 3D grid, as shown in Figure 4.4, thereby initiating the three-burst array calculations.

The initial three-dimensional mesh used to model the three-burst problem was substantially larger than that needed for simulating the two simultaneous bursts, as described in Section 4.2. This can be seen by comparing Figures 4.1 and 4.4. For the two-burst problem, both the x-z and y-z vertical coordinate planes were planes of symmetry for the problem. Thus, only a quarter space needed to be modeled for this problem. The three-burst calculation, however, had only one vertical plane of symmetry, namely the y-z plane, as shown in Figure 4.4. A larger region had to be modeled, therefore, for that problem.

The initial (x,y,z) grid for the 3D calculations, which were initiated at a problem time of 20ms, consisted of $100 \times 175 \times 150$ cubical cells, initially 2m on each side. This grid covered the $200\text{m} \times 350\text{m} \times 300\text{m}$ region (with 100m vertically in the ground below $z=0$) that was required to contain the wave fronts from the individual bursts just prior to interaction. The automatic expanding rezoner again was used to extend the initial 3D zoning as needed to follow the expanding shock fronts.

4.4 Three-Burst Array at 15m-DOB – Results

Figure 4.5 shows pressure contours at 100ms on a horizontal plane at 100m depth for three-burst problem. Peak pressures at that time and on that plane are $\sim 1\text{kb}$, and are occurring where shock fronts from the individual bursts overlap. Pressure contours on the vertical x-z coordinate plane are shown in Figure 4.5b.

Figure 4.6 shows corresponding results on the same planes at 250ms problem time. It can be seen from Figure 4.6b that the array is delivering 0.5kb ground shock stress to depths greater than 600m. Figure 4.7 shows footprints for the three-burst array on horizontal target planes at depths of ~ 250 and $\sim 500\text{m}$, while corresponding contours on the x-z and y-z vertical coordinate planes are shown in Figure 4.8. Note that the three-burst array produces a 0.5 kb footprint that covers an area of about one square kilometer and about one-half square kilometer, respectively, at the 250m and 500m depths. Again, these results can be compared directly with footprints from the two-burst calculations, as shown in Figure 4.3.

It is interesting to compare the three-burst footprints with results for a *single* 300kt burst at 15m-DOB, *i.e.*, a single burst with the same aggregated yield as delivered by the array. This comparison is shown in Figure 4.9 for planes at 250m and 500m depth. On the plane at 250m depth, the single burst and multiburst array give very comparable coverage at both the 0.5 and 1.0 kb levels. On the deeper (500m) plane, however, the 0.5 kb footprint from the multiburst array is considerably larger than that for the single burst. Also note that a sizeable (about 300 square meters) 1 kb footprint is produced at the 500m depth by the multiburst array; whereas, a single 300kt EPW cannot deliver

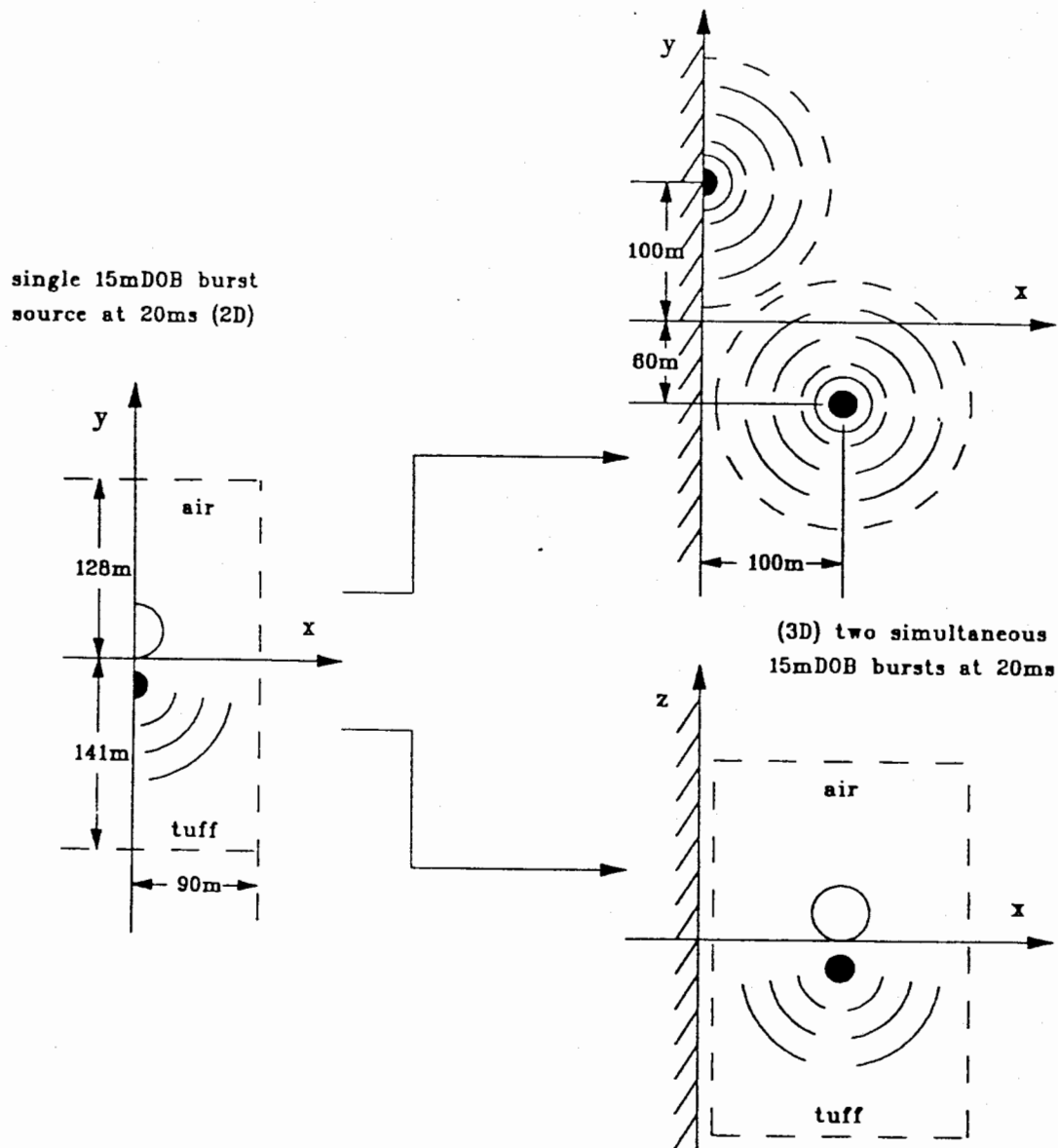


Figure 4.4. Use of Single-Burst Result (left) to Generate Starting Conditions (right) for 3D Calculations of Three, Simultaneous Bursts at 15m-DOB

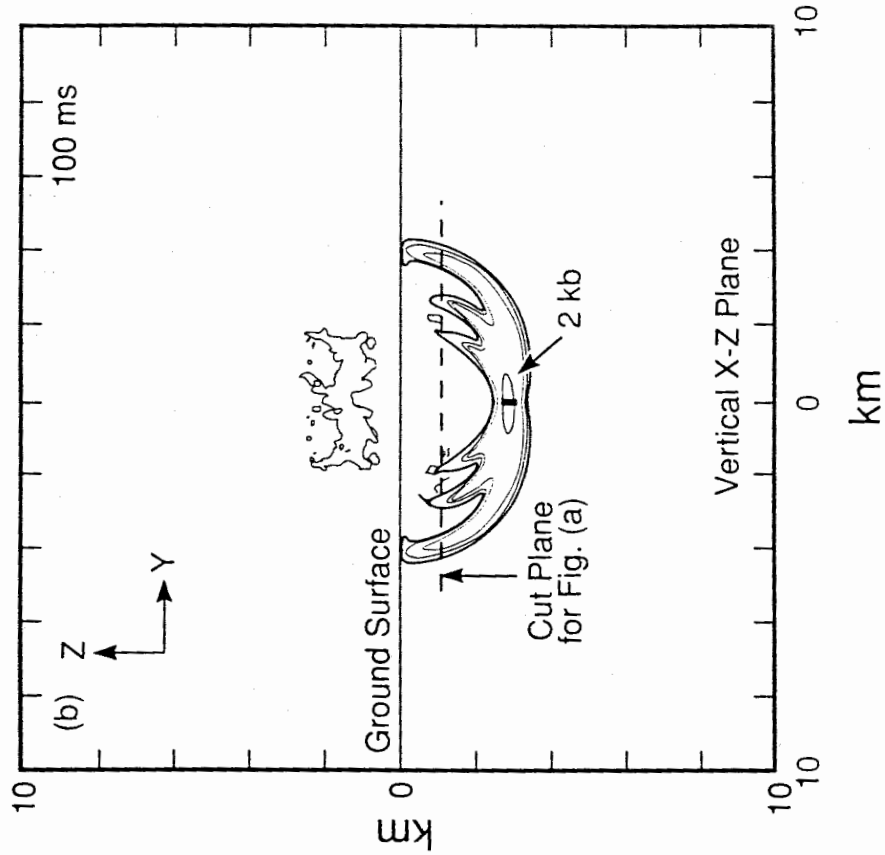
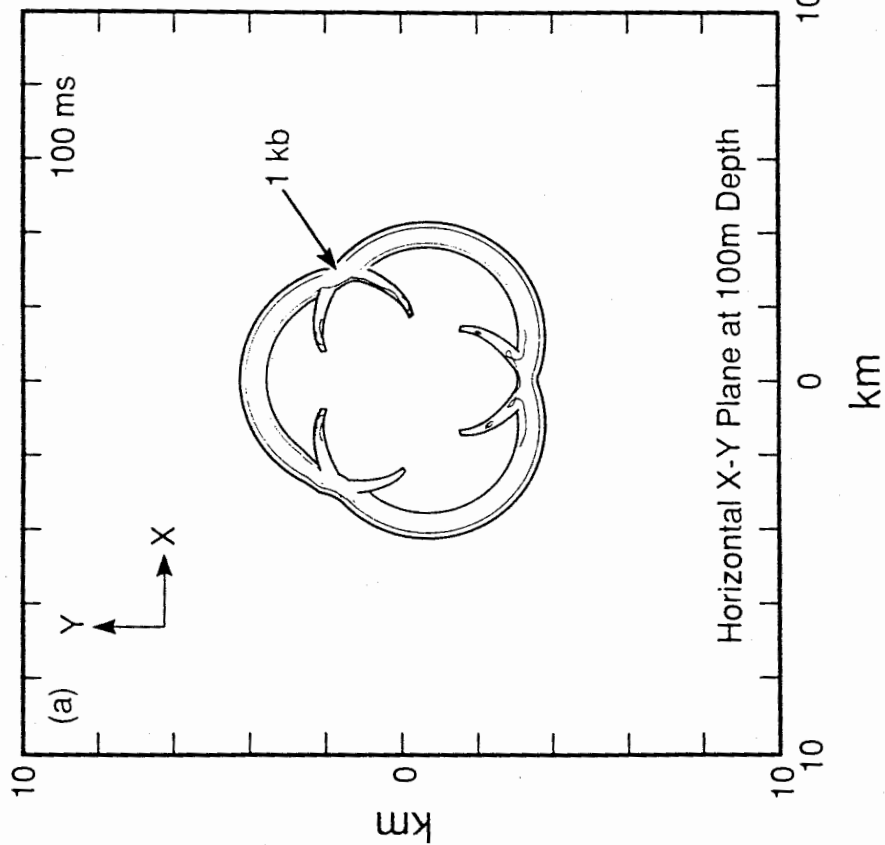


Figure 4.5 Pressure Contours at 100 ms for Three, Simultaneous, 100 kt Bursts at 15 m-DOB and 200 m Separation

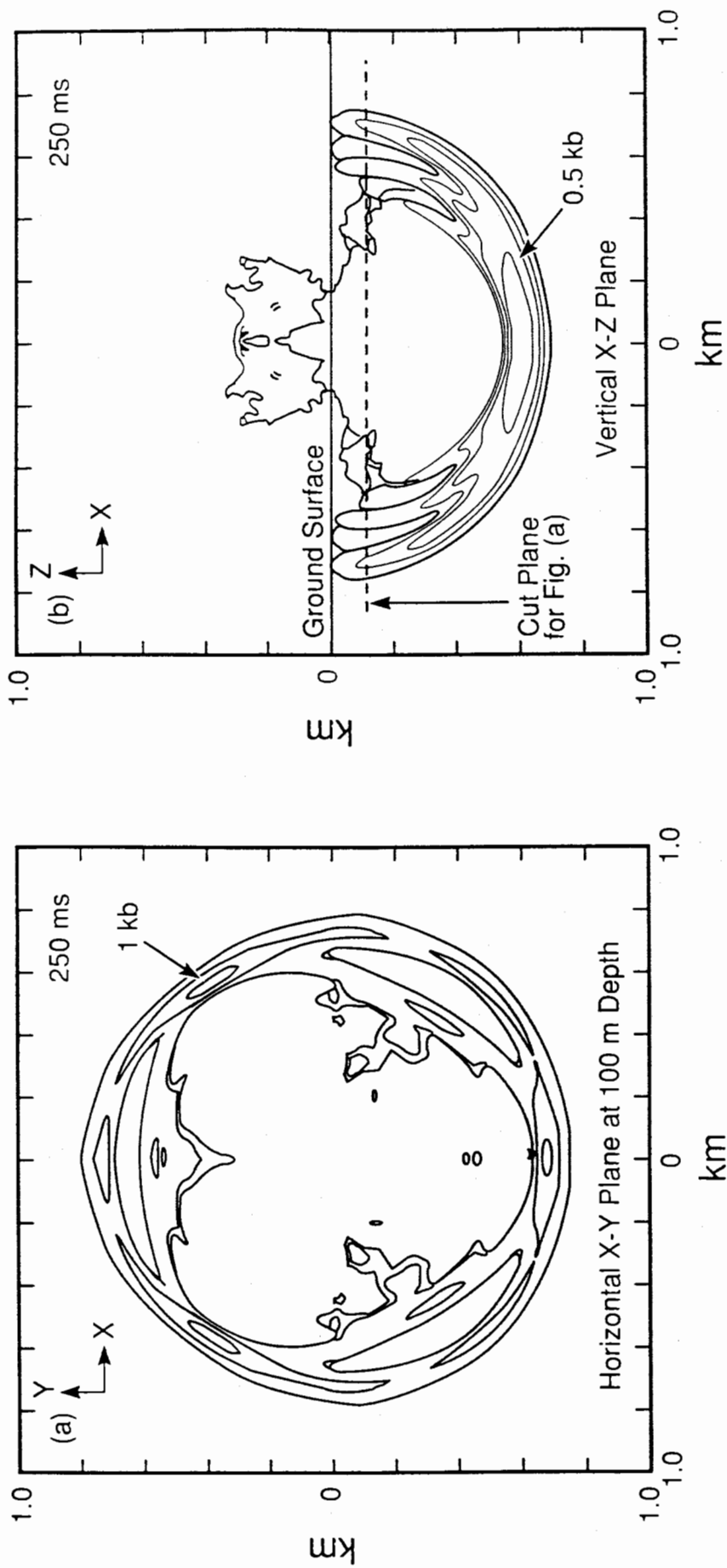


Figure 4.6 Pressure Contours at 250 ms for Three, Simultaneous, 100 kt Bursts at 15 m-DOB and 200 m Separation

1kb to that depth in the present target geology. These results would appear to support the idea that, with appropriate spacing and timing, a multiburst array of three 100kt EPWs can deliver equivalent, or stronger, ground shock effects to deeply-buried targets as a single EPW burst of the same aggregated yield.

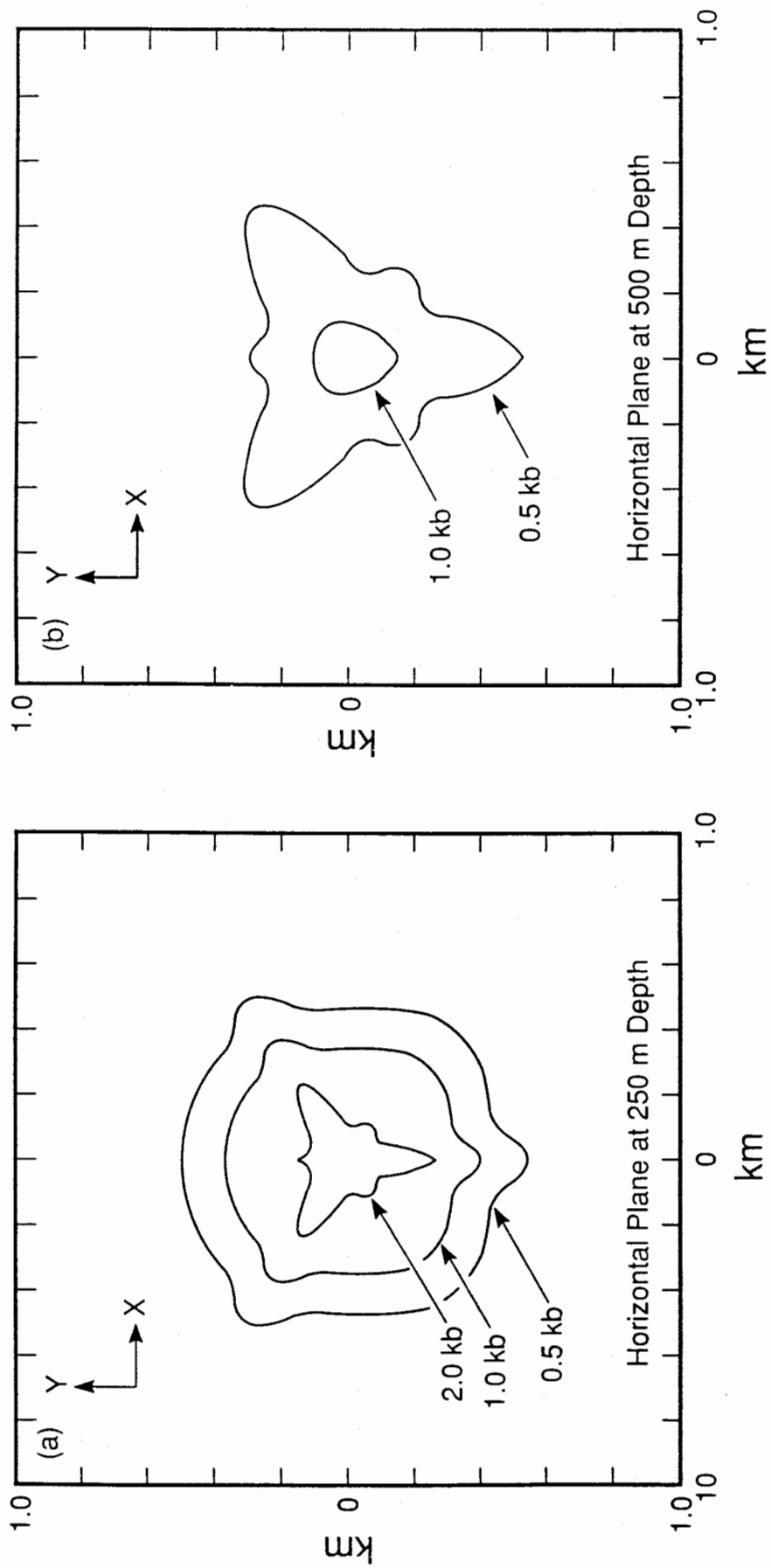


Figure 4.7 Peak Pressure Contours on Horizontal Planes for Three, Simultaneous, 100 kt Bursts at 15 m-DOB and 200 m Separation

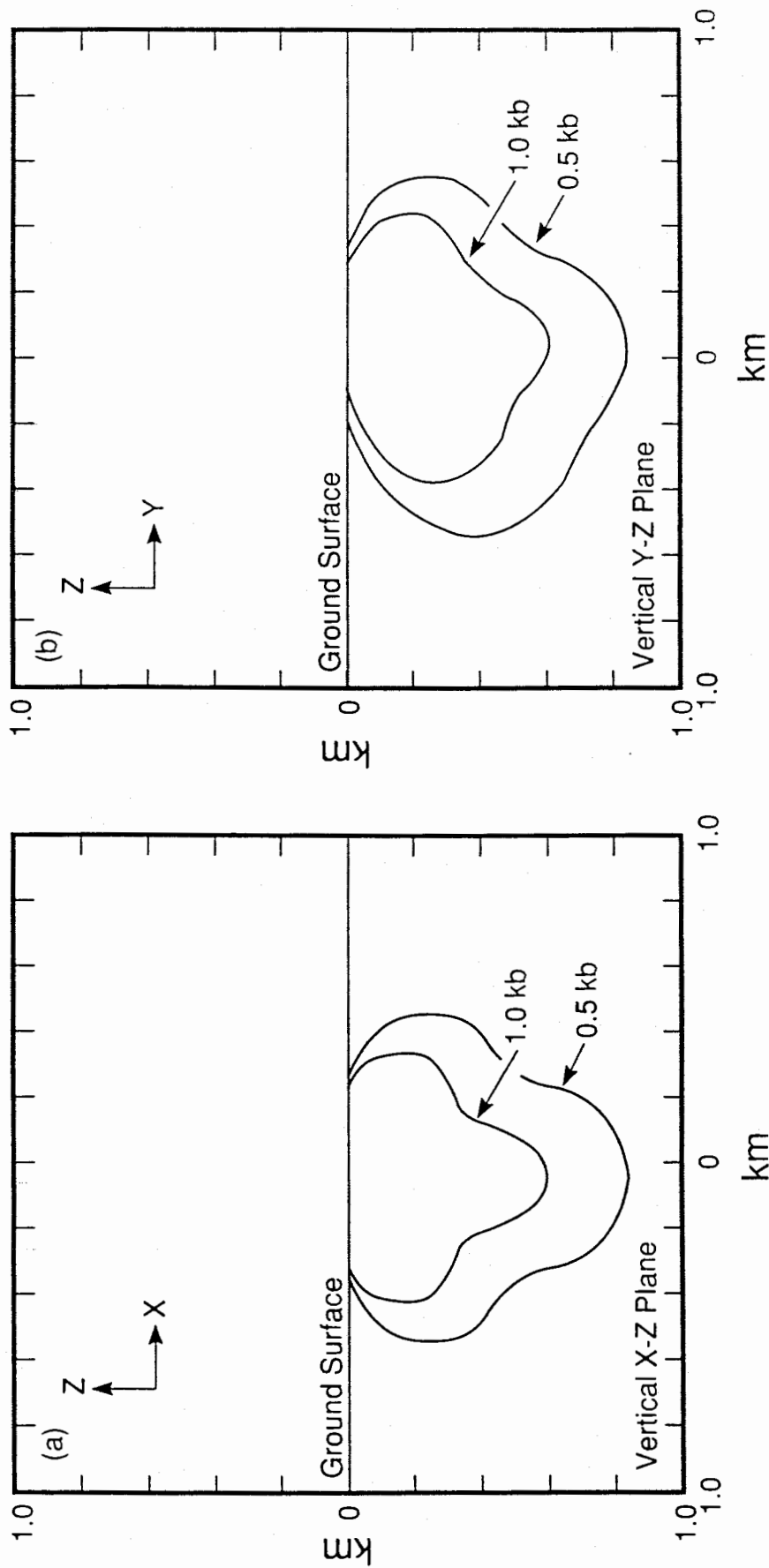


Figure 4.8 Peak Pressure Contours on Vertical Coordinate Planes for Three, Simultaneous, 100 kt Bursts at 15 m-DOB and 200 m Separation

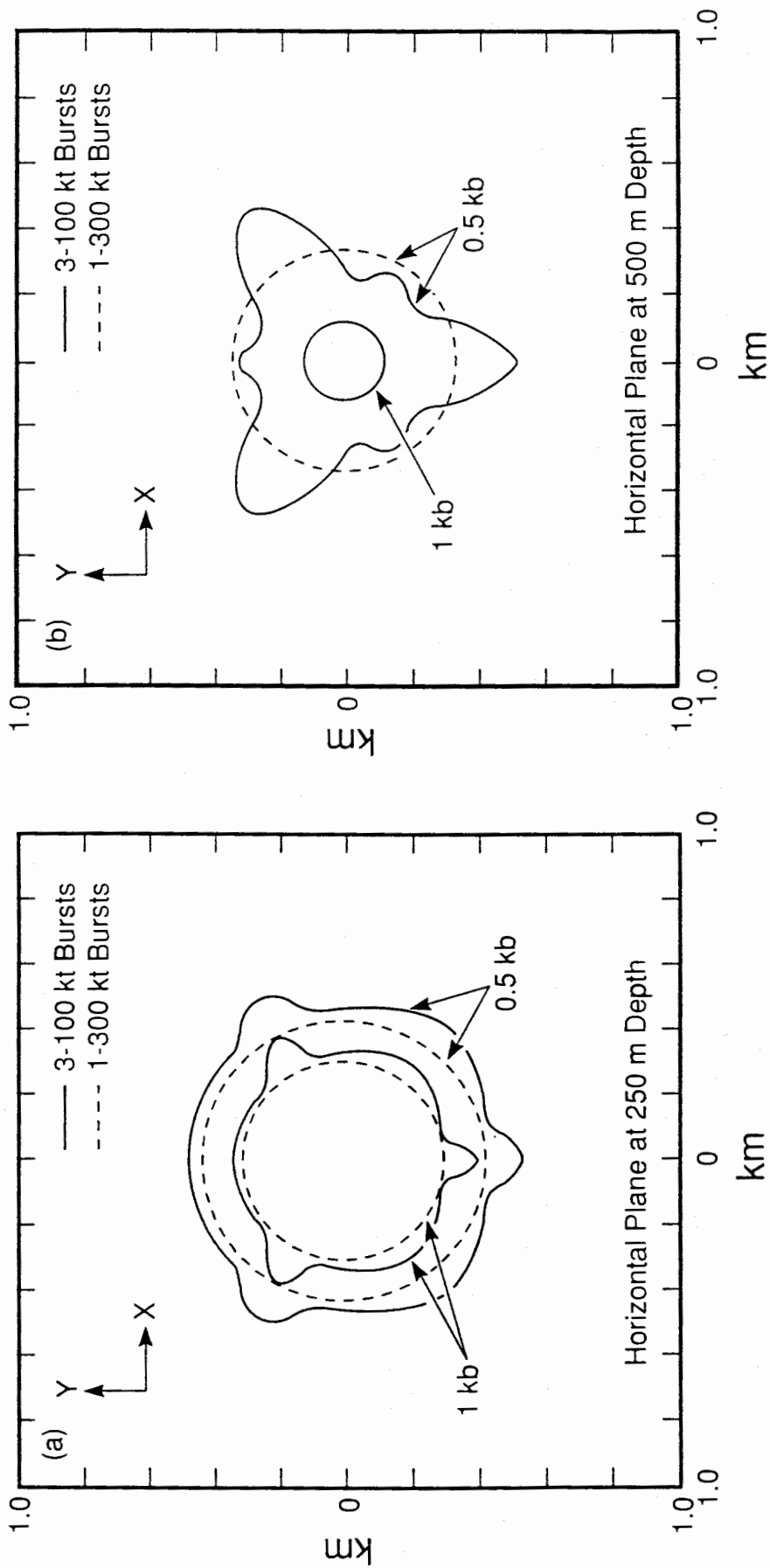


Figure 4.9 Peak Pressure Contours on Horizontal Planes. Comparison of Results for Three 100 kt Bursts and One 300 kt Burst

5. Discussion and Conclusions

This report presents results of two-dimensional and three-dimensional HULL hydrocode calculations of ground shock from simultaneous detonations of earth penetrator weapons (EPWs). The target was modeled as a homogeneous material, simulating wet, soft rock. The EPW arrays were assumed to be either two bursts, where depth, spacing, and timing were varied in the problems, or three bursts in an equilateral triangular pattern. Each weapon in the multiburst array was assumed to have a nominal yield of 100kt. For comparison with the multiburst results, calculations were also done for single EPW bursts of 200kt and 300kt yield.

Several different multiburst problems were simulated in this study. The first problem involved two fully-contained bursts. Different weapon spacings and variations in timing between the bursts were investigated. At most points in the target, there was sufficient delay between arrival of the disturbances from the two bursts that the ground shock effects of the bursts were independent. Thus, peak stress in these regions was no greater than that from a single burst. On the plane between the two bursts, however, and in a region on either side of that plane, superposition of the ground shock effects from the bursts produced a significant increase in peak stress over that from a single weapon. The size and geometry of that region of enhancement depended on the spacing and relative timing of the bursts. Analytical studies at Los Alamos National Laboratory, with which our results were compared, also show that shock speed in the target material influences the size and orientation of that region. Comparisons of the two-burst results with those for a single, 200kt fully-contained explosion show that, in the region of ground shock enhancement, the two-burst array delivers kilobar levels of peak stress to greater depths than does the 200kt burst. This advantage of the two-burst array, however, occurs in a relatively small region of the target.

Calculations were also done to simulate two-burst and three-burst arrays of 100kt EPWs at finite depth of burial. A 7m-DOB was used for the two burst problem, while a 15m-DOB was used for the three-burst array. The results of the two-burst, finite DOB calculations were qualitatively similar to those for the corresponding infinite DOB case, as described above. Due to effects of the proximate ground surface in the 7m-DOB calculations, the ground shock levels were lower at corresponding ranges from the burst than observed for the infinite DOB calculations, as would be expected. For the three-burst problem, the peak pressure footprints on deep horizontal planes in the target were found to be comparable to those from a single 300kt explosion at the same DOB. Thus these results support the notion that yield aggregation can be achieved by proper spacing and timing of smaller-yield EPW arrays.

We note, in conclusion, that results of the LANL linear superposition analyses, for the direction and extent of ground shock enhancement in the two-burst, infinite DOB problems, showed very good agreement with the hydrocode results. It has been seen in other Sandia analytical studies, as yet undocumented, as well as in similar work underway at other external organizations, that linear superposition methods give excellent agreement with hydrocode results for multiburst problems in which the geology is non-porous and homogeneous, and in which the ground shock stress levels of interest are in the range of a few kilobars or below. In such cases, therefore, superposition methods provide a computationally-efficient means for performing multiburst analyses. For more complex geologies, however, resort must be made to the fully-nonlinear capability of the hydrocode techniques to do the ground shock interaction analyses.

References

- [1] Yarrington, P., "Ground Shock from Earth Penetrator Bursts," SAND88-1497, 11/88. ovo
- [2] D. A. Matuska and J. J. Osburn, "HULL Documentation Volume I: Technical Discussion; Volume II: Users Manual", Orlando Technology, Inc., Shalimar, Florida, October 1987.
- [3] Demuth, R. B., L. G. Margolin, B. D. Nichols, T. F. Adams, and B. W. Smith, "SHALE: A Computer Program for Solid Dynamics," Los Alamos National Laboratory Report, LA-10236, May 1985.
- [4] B. C. Trent, "Numerical Simulation of the Simultaneous Detonation of Two Identical, Fully Contained Explosions", Los Alamos National Laboratory Report LA-11294-MS, July 1989. ✓
- [5] G. P. DeVault and B. C. Trent, "Two-Dimensional Multiburst Calculations with the SHALE Code", Los Alamos National Laboratory Report LA-11835-MS, July 1990.

Appendix A

Results Archival

The calculations in this study were done with version 122 of HULL [2]. A number of change decks are either required to run on the Sandia CRAY/CTSS system, or are used to correct code errors and add new code features. The change decks used for a given calculation are saved and available as part of the standard output stored on the SNL Integrated File System (IFS), as discussed below. For reference, the origination time and storage location for the code and change deck versions used are saved in the CCL log file.

The only nonstandard change deck used for the present studies was one implementing a modified automatic rezoner. This change deck is listed on the archival output files, as discussed above, and is also provided on the microfiche listing attached to this report, for easier reference. The automatic rezoning logic in the HULL program, in both two- and three-dimensional form, was entirely rewritten for these analyses, in large part to ensure that both two- and three-dimensional analyses used exactly the same rezone scheme. The translating rezone option was modified to always shift an integral number of cells, with exact preservation of information between rezoning. The expanding rezone option was modified to include a very simple "anti-diffusion" correction to prevent multiple rezones from significantly diffusing the undisturbed ground surface (also applicable to preserving subsurface layering, if present). Both rezoning options were modified to introduce the correct ambient material in new mesh regions, *i.e.*, air above ground surface and tuff below, in this case.

A number of calculations were done for this multiburst ground shock effects study. All output files are stored in the IFS directory /e00021674/hull2-2burst. Sample input decks can be found in the subdirectory: input-files, and one sample input deck is provided in the microfiche listing attached to this report. The other subdirectories contain:

Subdirectory	Contents
2d-infdob	2D, fully-contained, two-100kt-burst array analyses
2d-7mdob	2D, 7m-DOB, single-100kt-burst calculation
2d-15mdob	2D, 15m-DOB, single-100kt-burst calculation
3d-7mdob	3D, 7m-DOB, two-100kt-burst calculation
3d-15mdob	3D, 15m-DOB, three-100kt-burst calculation

The results of any given run (depending on the set of KEEL, HULL, PULL and STATIONS calculations performed) can include the following:

Filename	Description
hul4{id}{suf}{com}	binary plot/restart file
hul9{id}{suf}{com}	binary time history file

(where {id} is a one-character job identifier, {suf} is the CTSS suffix, and {com} is a nine-or-less character comment) as well as two or more of the ASCII output files:

Filename	Contents
outk{id}{suf}{com}	concatenated PLANK input/output, SAIL input/output and KEEL input/output
outck{id}{suf}{com}	change decks used in KEEL run
ship{id}{suf}{com}	concatenated PLANK input/output, SAIL input/output and HULL input
hout{id}{suf}{com}	HULL output
outch{id}{suf}{com}	change decks used in HULL run
outp{id}{suf}{com}	concatenated PLANK input/output, SAIL input/output and PULL input/output
outcp{id}{suf}{com}	change decks used in PULL run
outs{id}{suf}{com}	concatenated PLANK input/output, SAIL input/output and STATIONS input/output
outcs{id}{suf}{com}	change decks used in STATIONS run
lokh{id}{suf}{com}	CCL log file for entire run

Sandia Internal:

1510 J. C. Cummings
1540 J. R. Asay
1541 J. M. McGlaun
1542 P. Yarrington (10)
1542 A. F. Farnsworth
1543 P. L. Stanton
1544 J. R. Asay, Actg.
1545 D. R. Martinez
1550 C. W. Peterson
3141 S. A. Landenberger (5)
3151 G. C. Claycomb (3)
5160 G. R. Otey
5161 J. A. Andersen
5165 J. M. Freeman
5166 R. C. Hartwig
5166 A. B. Cox
5167 D. F. McVey
5167 J. K. Shane
6410 D. A. Dahlgren
6418 S. L. Thompson
6418 L. N. Kmetyk (10)
7213 J. D. Saylor
8170 J. W. Hickman
8171 C. T. Oien
8241 L. E. Voelker
8242 M. R. Birnbaum
8523 R. C. Christman (Library)
9010 W. C. Hines
9013 W. H. Ling
9120 M. M. Newsom

[REDACTED]